



1 **Multiple pathways for the formation of secondary organic aerosol in North China Plain**  
2 **in summer**

3 Yifang Gu<sup>1,4</sup>, Ru-Jin Huang<sup>1,2,3,4</sup>, Jing Duan<sup>1</sup>, Wei Xu<sup>1</sup>, Chunshui Lin<sup>1</sup>, Haobin Zhong<sup>1,4</sup>, Ying  
4 Wang<sup>1</sup>, Haiyan Ni<sup>1</sup>, Quan Liu<sup>5</sup>, Ruiguang Xu<sup>6,7</sup>, Litao Wang<sup>6,7</sup>, Yong Jie Li<sup>8</sup>

5 <sup>1</sup>SKLLQG, Center for Excellence in Quaternary Science and Global Change, Institute of Earth  
6 Environment, Chinese Academy of Sciences, Xi'an 710061, China

7 <sup>2</sup>Open Studio for Oceanic-Continental Climate and Environment Changes, Pilot National  
8 Laboratory for Marine Science and Technology (Qingdao), Qingdao 266000, China

9 <sup>3</sup>Institute of Global Environmental Change, Xi'an Jiaotong University, Xi'an 710049, China

10 <sup>4</sup>University of Chinese Academy of Sciences, Beijing 100049, China

11 <sup>5</sup>State Key Laboratory of Severe Weather & Key Laboratory of Atmospheric Chemistry of C  
12 MA, Chinese Academy of Meteorological Sciences, Beijing 100081, China

13 <sup>6</sup>Department of Environmental Engineering, School of Energy and Environmental Engineering,  
14 Hebei University of Engineering, Handan 056038, China

15 <sup>7</sup>Hebei Key Laboratory of Air Pollution Cause and Impact, Handan 056038, China

16 <sup>8</sup>Department of Civil and Environmental Engineering, and Centre for Regional Oceans, Faculty  
17 of Science and Technology, University of Macau, Taipa, Macau 999078, China

18 *Correspondence to:* Ru-Jin Huang ([rujin.huang@ieecas.cn](mailto:rujin.huang@ieecas.cn))

19

20



21 **Abstract**

22 Secondary organic aerosol (SOA) has been identified as a major contributor to fine  
23 particulate matter (PM<sub>2.5</sub>) in North China Plain (NCP). However, the chemical mechanisms  
24 involved are still unclear due to incomplete understanding of its multiple formation processes.  
25 Here we report field observations in summer in Handan of NCP, based on high-resolution  
26 online measurements. Our results reveal the formation of SOA via photochemistry and two  
27 types of aqueous-phase chemistry, the latter of which include nocturnal and daytime processing.  
28 The photochemical pathway is the most important under high O<sub>x</sub> (=O<sub>3</sub> + NO<sub>2</sub>) conditions (65.1  
29 ± 20.4 ppb). The efficient SOA formation from photochemistry (phochem-SOA) dominated the  
30 daytime (65% to OA) with an average growth rate of 0.8 μg m<sup>-3</sup> h<sup>-1</sup>. During the high relative  
31 humidity (RH: 83.7 ± 12.5 %) period, strong nocturnal aqueous-phase SOA formation (aq-SOA)  
32 played a significant role in SOA production (45% to OA) with a nighttime growth rate of 0.6  
33 μg m<sup>-3</sup> h<sup>-1</sup>. Meanwhile, an equally fast growth rate of 0.6 μg m<sup>-3</sup> h<sup>-1</sup> of phochem-SOA from  
34 daytime aqueous-phase photochemistry was also observed, which contributed 39% to OA,  
35 showing that photochemistry in the aqueous phase is also a non-negligible pathway in summer.  
36 The primary-related-SOA (SOA attributed to primary particulate organics) and aq-SOA are  
37 related to residential coal combustion activities, supported by distinct fragments from  
38 polycyclic aromatic hydrocarbons (PAHs). Moreover, the conversion and rapidly oxidation of  
39 primary-related-SOA to aq-SOA could be possible in the aqueous phase under high-RH  
40 conditions. This work sheds light on the multiple formation pathways of SOA in ambient air of  
41 complex pollution, and improves our understanding of ambient SOA formation and aging in  
42 summer with high oxidation capacity.

43

44 **KEYWORDS:** secondary organic aerosol, aqueous-phase chemistry, photochemistry,  
45 multiple-phase chemistry, complex air pollution

46



## 47 1. Introduction

48 Rapid economic growth and urbanization processes have led to severe particulate air  
49 pollution in China, affecting air quality, climates and human health (Huang et al., 2014;  
50 Cohen et al., 2017; An et al., 2019). Organic aerosol (OA) is a major component of aerosol  
51 particles, consisting of 20-90% of fine particle mass (Jimenez et al., 2009; Zhang et al., 2011).  
52 OA is either emitted directly from primary sources (referred to as primary OA, POA) such as  
53 traffic, cooking, coal combustion, and biomass burning, or produced through gas-to-particle  
54 conversion (referred to as secondary OA, SOA) in the atmosphere. In recent years, with the  
55 implementation of control measures, the POA fraction is decreasing and SOA fraction is  
56 increasing in North China Plain (NCP), indicating that SOA is becoming more critical for urban  
57 air quality (Huang et al., 2019; Xu et al., 2019; Gu et al., 2020). However, our understanding  
58 of the formation mechanisms and evolution processes of SOA is still limited.

59 Generally, SOA can be formed through gas-phase photochemical oxidation of volatile  
60 organic compounds (VOCs) followed by nucleation or condensation of oxidation products onto  
61 the preexisting particles (Donahue et al., 2006). Herndon et al., (2008) showed that oxygenated  
62 organic aerosol (OOA), a surrogate of SOA, was well correlated with odd oxygen ( $O_x = O_3 +$   
63 nitrogen dioxide ( $NO_2$ )) during photochemical processing. SOA can also be formed in the  
64 aqueous phase on wet aerosols, clouds and fogs through further chemical processes of water-  
65 soluble organic compounds or organic products of gas-phase photochemistry (Ervens et al.,  
66 2011, 2014). A growing number of laboratory studies and field measurements have indicated  
67 that aqueous-phase processes contribute efficiently to the formation of SOA (Gilardoni et al.,  
68 2016; Bikkina et al., 2017). However, how photochemistry and aqueous-phase chemistry  
69 coordinate to affect the formation of SOA is still unclear, despite numerous measurements to  
70 explore this question using aerosol chemical speciation monitor (ACSM) or aerosol mass  
71 spectrometer (AMS) (Hu et al., 2016b; Hu et al., 2017; Sun et al., 2016; Li et al., 2017; Sun et  
72 al., 2018b; Huang et al., 2019; Gu et al. 2020; Kuang et al., 2020). Field measurements in  
73 Beijing suggested that gas-phase photochemical oxidation can play a dominant role in SOA  
74 formation (Sun et al., 2016; Hu et al., 2016a). Xu et al., (2017) showed that less oxidized-OOA  
75 (LO-OOA) was mainly formed through photochemical oxidation, while the more oxidized-  
76 OOA (MO-OOA) formation was dominantly formed by aqueous-phase chemistry in Beijing  
77 for different seasons. Kuang et al. (2020) investigated the effects of gas-phase and aqueous-  
78 phase photochemical processes on the formation of SOA and found that photochemical  
79 aqueous-phase SOA formation dominantly contributed to daytime OOA formation in winter  
80 Gucheng, located between Beijing (~100 km) and Baoding (~40 km) on the NCP. We found  
81 that photochemical processing attributed mostly to MO-OOA in summertime Beijing (Gu et al.,  
82 2020). Although these studies provided important insights into SOA formation processes, our  
83 understanding on the photochemical and aqueous-phase formation pathways for SOA and their



84 impacts on oxidation degree are far from complete. This lack of understanding is especially so  
85 under the conditions that atmospheric oxidative capacity and pollution characteristics have been  
86 largely changing in China due to large reduction in direct emissions of air pollutants.

87 In this study, we investigated the photochemical versus aqueous-phase processing for SOA  
88 composition and oxidation degree of OA in summertime Handan, which is a typical  
89 industrialized city in the NCP region. The city is located at the intersectional area of Hebei,  
90 Shanxi, Henan, and Shandong—four heavily urbanized and industrialized provinces (Fig. S1),  
91 and it is therefore an ideal site to investigate the SOA formation pathways in the NCP region.  
92 The multiple formation pathways, evolution of SOA composition, and oxidation degree under  
93 different meteorological conditions were discussed, which sheds light on the aqueous-phase  
94 chemistry and photochemical processing in SOA formation in the NCP region of China.

## 95 **2. Experimental methods**

### 96 **2.1 Sampling site**

97 Measurements were conducted from 10<sup>th</sup> August 2019 to 17<sup>th</sup> September 2019 on the campus  
98 of Hebei University of Engineering (36.57 °N, 114.50 °E), located at the southeast edge of urban  
99 Handan (Fig. S1). The site is surrounded by a school and residential areas, ~300 m north to  
100 South Ring Road and ~400 m northeast to the Handan Highway (S313). The sampling site is  
101 on the rooftop of a four-floor building, approximately 12 m above the ground.

### 102 **2.2 Instrumentation**

103 Real-time non-refractory PM<sub>2.5</sub> composition was measured by a soot particle long time-of-  
104 flight aerosol mass spectrometer (SP-LToF-AMS, Aerodyne Research Inc.) with a time  
105 resolution of 1 min. The detailed instrument description and operation of AMS were reported  
106 in Onasch et al., (2012). Compared to the conventional AMS, the LToF mass analyzer can  
107 provide much better mass resolution of ~8000. During the campaign, the instrument was  
108 operated in the “laser off” mode and only the standard tungsten vaporizer was applied.  
109 Therefore, only non-refractory PM<sub>2.5</sub> components (NR-PM<sub>2.5</sub>) were measured, including  
110 organics (Org), nitrate (NO<sub>3</sub>), sulfate (SO<sub>4</sub>), ammonium (NH<sub>4</sub>), and chloride (Cl). Ambient  
111 air was sampled and dried by a Nafion dryer (MD-700-24S, Perma Pure, Inc.) at a flow rate of  
112 5 L min<sup>-1</sup>, and then sub-sampled into the SP-LToF-AMS at a flow rate of ~ 0.1 L min<sup>-1</sup>. An  
113 aerodynamic PM<sub>2.5</sub> lens was used to focus the particle into a beam, which was then impacted  
114 on the heated tungsten surface (~ 600 °C) and flash-vaporized. Electron ionization with 70 eV  
115 was used to ionize the vaporized gases. The ionization efficiency (IE) and the relative ionization  
116 efficiency (RIE) calibrations (Jimenez et al., 2003) were conducted by using 350 nm  
117 ammonium nitrate (NH<sub>4</sub>NO<sub>3</sub>) and ammonium sulfate ((NH<sub>4</sub>)<sub>2</sub>SO<sub>4</sub>) particles.



118 Gaseous pollutants including SO<sub>2</sub> (9850 SO<sub>2</sub> analyzer, Ecotech), NO<sub>2</sub> (Model 42i NO-NO<sub>2</sub>-  
119 NO<sub>x</sub> analyzer, Thermo Scientific), CO (Model 48i carbon monoxide analyzer, Thermo  
120 Scientific), O<sub>3</sub> (Model 49i ozone analyzer, Thermo Scientific), and meteorological parameters  
121 including RH and temperature were also measured during the observation period. Furthermore,  
122 an aethalometer (Model AE-33, Magee Scientific) was deployed to measure the mass  
123 concentration of black carbon (BC) at a time resolution of 1 min.

### 124 **2.3 Data Analysis**

125 The data analysis software (SQUIRREL, version 1.63I and PIKA, 1.23I) within Igor Pro 6.37  
126 (WaveMetrics) was used to analyze the AMS data. The experimental RIE values of 4 (NH<sub>4</sub>)  
127 and 1.2 (SO<sub>4</sub>) and the standard RIE values of 1.4 (Org), 1.1 (NO<sub>3</sub>) and 1.3 (Chl) were used.  
128 The composition-dependent collection efficiency (CDCE, Middlebrook et al., 2012) was used  
129 to compensate for the incomplete detection caused by particle bounce on the vaporizer. An  
130 improved Ambient (I-A) method was adopted for the elemental ratio analysis of high-resolution  
131 (HR) OA mass spectra, such as oxygen-to-carbon (O:C), and hydrogen-to-carbon (H:C) ratios  
132 (Canagaratna et al., 2015), which reflect the relative composition and oxidation degree for  
133 different OA source. In our study, PMF was performed on HR mass spectra of OA for ions with  
134  $m/z$  values of 12-120, together with the signals from integer  $m/z$  values between 121 to 300 (i.e.,  
135 unit mass resolution, UMR) using SoFi (version 6.3) in Igor Pro (Paatero, 1999; Canonaco et  
136 al., 2013). The data and error matrices were preprocessed according to Elser et al., (2016) and  
137 detailed description of PMF analysis was given elsewhere (Canonaco et al. 2013; Elser et al  
138 2016). Unconstrained PMF solutions with varied factor numbers were analyzed and six factors  
139 were resolved, including two primary and four secondary organic factors (Fig. 3). The six-factor  
140 solution was preferred because the five-factor solution was not able to separate high signal of  
141  $m/z$  44 (which represents high oxidation state) from primary organic aerosol (POA) factors,  
142 while the seven-factor solution added additional OOA factors with similar profiles and noisy  
143 time series for which no physical interpretation could be found. The two POA factors consisted  
144 of a traffic-related factor (hydrocarbon-like OA, HOA) and a cooking-related factor (COA),  
145 which had been resolved in previous summer studies in NCP (Elser et al., 2016; Hu et al., 2016b;  
146 Sun et al., 2016; Huang et al., 2019). AMS source apportionment studies often report one or  
147 two oxygenated organic aerosol (OOA) factors that are distinguished by the extent of  
148 oxygenation and linked to volatility or oxidation degree. Owing to higher mass resolution of  
149 LTOF-AMS and the inclusion of integer-mass signals for  $m/z$  from 121 to 300 for high-  
150 molecular-weight species such as polycyclic aromatic hydrocarbons (PAHs), we herein  
151 resolved four SOA factors. These four SOA factors include aq-SOA attributable to aqueous-  
152 phase chemistry, phochem-SOA attributable to photochemistry, primary-related-SOA  
153 attributable to prompt oxidation of POA during emission, and fresh-SOA with a lower  $f_{44}/f_{43}$   
154 ratio (fraction of  $m/z$  44 and 43 in OA).



## 155 2.4 Aerosol liquid water content

156 The aerosol liquid water content (ALWC) was simulated by ISORROPIA-II model  
157 (Fountoukis and Nenes, 2007; Hennigan et al., 2015) using the measurements of ambient  
158 inorganic species (NO<sub>3</sub>, SO<sub>4</sub>, NH<sub>4</sub>, and Chl) and meteorological parameters (temperature and  
159 RH). The simulation was run in “metastable” mode where all components are assumed to be  
160 deliquescent and contain no solid matter. The concentrations and speciation (if dissociated) of  
161 those inorganic species in thermodynamic equilibrium was then simulated by the model and  
162 then the ALWC was calculated. The ISORROPIA-II model does not consider the contribution  
163 to ALWC from organics, since inorganic aerosols dominate the water uptake by ambient  
164 particles with a contribution of approximate >80% of the total ALWC (Huang et al., 2020).

## 165 3. Results and discussion

### 166 3.1 SOA sources

167 In our study, SOA accounted for 69% (13.5  $\mu\text{g m}^{-3}$ ) of the total OA (19.6  $\mu\text{g m}^{-3}$ ),  
168 representing the dominant fraction in OA in summer Handan. Among the four PMF-resolved  
169 SOA sources (Fig. 1), phochem-SOA dominated (31% to total OA), followed by fresh-SOA  
170 (18%), aq-SOA (15%), and primary-related-SOA (5%). Since we focus on SOA formation in  
171 this study, detailed descriptions of the HOA (12%) and COA (19%) is provided in section 1.1  
172 in the SI. The mass spectral profiles of the six OA source factors are shown in Fig. 1, while the  
173 time series of the SOA factors are shown in Fig. 2. In particular, a remarkable continuous  
174 growth of aq-SOA concentration (from  $\sim 0.3 \mu\text{g m}^{-3}$  to  $25.2 \mu\text{g m}^{-3}$ ) and ALWC (from  $3.1 \mu\text{g m}^{-3}$   
175 to  $486.1 \mu\text{g m}^{-3}$ ) occurred on 24<sup>th</sup>-28<sup>th</sup> August (Fig. 2d). Meanwhile, the O:C ratio indicative  
176 of OA oxidation state displayed a continuous increase from 0.52 to a maximum of 0.93 during  
177 this time (Fig. 2e), consistent with the continuous increase in RH (reaching over 95%). This  
178 observation hints that during this period aqueous-phase processing might have played an  
179 important role in aq-SOA formation. This role of aqueous-phase processing in SOA formation  
180 is not just specific to this particular event, but also important in the whole campaign, which is  
181 discussed in detail in section 3.3 later.

182 To further investigate the SOA formation mechanism, the dataset was segregated into three  
183 periods according to different features depends on meteorological parameters (Fig. 2), i.e., the  
184 reference period (P1), high-O<sub>x</sub> period (P2) and high-RH period (P3). Briefly, the reference  
185 period, P1, was characterized by a low average OA concentration ( $15.4 \pm 3.2 \mu\text{g m}^{-3}$ ) and was  
186 mainly affected by clean air from southwest of the sampling site and precipitation activities  
187 (Table S1). The high-O<sub>x</sub> period (P2) was featured by a high O<sub>x</sub> concentration ( $65.1 \pm 20.4$  ppb),  
188 warmer temperatures ( $26.4 \pm 4.0$  °C) but lower RH ( $57.7 \pm 17.5$  %). The mass loadings of OA  
189 ( $19.8 \pm 4.7 \mu\text{g m}^{-3}$ ) and other pollutants in P2 were higher than those in P1 (Table S1). P3 was



190 assigned as a high-RH period because of the noticeably high RH ( $83.7 \pm 12.5 \%$ ) and high  
191 ALWC ( $95.4 \pm 114.2 \mu\text{g m}^{-3}$ ). Winds were weak ( $<1.0 \text{ m s}^{-1}$ ) throughout this period, indicative  
192 of stagnant conditions, which facilitated pollutant accumulation and resulted in the highest  
193 average OA concentrations ( $25.0 \pm 6.2 \mu\text{g m}^{-3}$ ).

194 During the reference period (P1), SOA had the lowest contribution to OA (57%), and the  
195 photochem-SOA and aq-SOA constituted 22% and 21% to total OA, respectively. For the high-  
196  $\text{O}_x$  period (P2), enhanced SOA formation was found, with the SOA fraction increased to 71%  
197 of the total OA. The photochem-SOA showed the highest mass loading of  $7.3 \mu\text{g m}^{-3}$  and highest  
198 contribution of 37% to total OA. These increases suggest that high- $\text{O}_x$  condition facilitates the  
199 production of SOA by photochemistry, making the photochem-SOA the major source of SOA  
200 during P2. During the high-RH period (P3), SOA fraction continually increased, approaching  
201 79% in total OA, and the SOA was mainly contributed by aq-SOA and fresh-SOA. The mass  
202 contribution of aq-SOA increased dramatically from 9% to total OA during P2 to 33% during  
203 P3 (Fig. S2), and average mass concentrations from  $1.8 \mu\text{g m}^{-3}$  to  $8.3 \mu\text{g m}^{-3}$ , which suggests  
204 rapid SOA production through the aqueous-phase chemistry. Comparatively, the contribution  
205 of fresh-SOA was about ~20% in both P2 and P3, but lower in P1 (9%), suggesting that the  
206 formation fresh-SOA was effected by both high  $\text{O}_x$  and high RH. It should also be noted that  
207 O:C ratio increased in the succession from P1 (0.73) to P2 (0.74) and further to P3 (0.77),  
208 accompanied by continually decrease of H:C ratio from 1.64 to 1.56, and to 1.53 (Fig. 3),  
209 suggesting the increase of OA oxidation degree. As a result, the high  $\text{O}_x$  in P2 and high RH in  
210 P3 (as compared to P1) promoted the formation of SOA, specifically photochem-SOA (in P2)  
211 and aq-SOA (in P3), leading to the increase in the degree of oxygenation in total OA.

212 Although the primary-related-SOA constituted a small fraction and showed little variation  
213 during P1~P3 (3%~5%), this SOA source is also of particular interest because of its distinctive  
214 fragments with high  $m/z$  values in the mass spectrum (Fig. 1d). At  $m/z < 120$ , the primary-  
215 related-SOA had higher intensities for  $m/z$  43 (mainly  $\text{C}_2\text{H}_3\text{O}^+$ ) and  $m/z$  44 (mainly  $\text{CO}_2^+$ ) than  
216 those in POA, indicating a typical nature of less-oxidized SOA. At  $m/z > 120$ , PAH-derived  
217 fragments are clearly evident in the mass spectrum of the primary-related-SOA, as indicated by  
218 PAH-like ions at  $m/z$  152, 165, 178, 189, 202, 216, 226 + 228, 240 + 242, 250 + 252, 264 +  
219 266, and 276 + 278 (Dzepina et al., 2007). Previous AMS studies have observed pronounced  
220 peaks of PAH ions in POA mass spectra, such as those in coal combustion organic aerosol  
221 (CCOA) and biomass burning organic aerosol (BBOA) (Hu et al., 2016b; Zhao et al., 2019),  
222 but rarely in SOA. This observation implies that the primary-related-SOA may be related to the  
223 POA originated from domestic coal combustion (Xu et al., 2006). Moreover, this SOA factor  
224 exhibited relatively better correlations with some gaseous pollutants (Fig. S4), such as CO ( $R$   
225 = 0.6) and  $\text{NO}_2$  ( $R$  = 0.5), and also tracked with HOA ( $R$  = 0.4). These observations suggest  
226 that the primary-related-SOA might be transformed from locally emitted POA as a non-



227 negligible source to SOA. Overall, our results suggest that SOA could be formed through  
228 different pathways, in particular photochemistry, aqueous-phase chemistry, and conversion of  
229 POA to SOA contributed to SOA formation.

### 230 3.2 Photochemistry

231 As expected for summertime, photochemistry associated with  $O_x$  has significant impacts on  
232 the formation and evolution of SOA. Herein, the relationships between OA factors and  $O_x$  were  
233 investigated to offer insights into the formation mechanisms of SOA associated with the ozone  
234 production chemistry (Herndon et al., 2008). During P2, as  $O_x$  increased, the mass loadings of  
235 phochem-SOA showed a substantially increasing trend when  $O_x$  was  $> 30$  ppb and eventually  
236 saturated when  $O_x$  was  $>100$  ppb, raising the contribution of phochem-SOA from 20% to 61%  
237 of total OA (Fig. 4). This observation indicates the importance of photochemistry in the  
238 formation of phochem-SOA in summer, in which high  $O_x$  concentration as well as temperature  
239 corresponding to strong atmospheric oxidative capacity, can accelerate the photochemical  
240 formation (Duan et al., 2021). As a comparison, the mass concentrations of other OA factors  
241 except phochem-SOA showed decreasing trends as  $O_x$  increased (Fig. 4c). Such differences  
242 between SOA factors are likely due to the enhanced secondary production/transformation from  
243 POA and fresher SOA factors to the more aged phochem-SOA. Note that the O:C ratio  
244 presented a faster increasing rate as a function of  $O_x$  (from 0.6 to 1.0, Fig. 4d) than those in P1  
245 and P3, suggesting that photochemistry resulted in higher OA oxidation state during P2.

246 The average diurnal variations of SOA factors, O:C ratios,  $O_x$ , temperature, and RH during  
247 different periods are shown in Fig. 6 and Fig. S7. During P2, phochem-SOA was produced  
248 quickly and played the dominant role during daytime, while its concentration typically  
249 decreased during nighttime. The average concentration of phochem-SOA increased continually  
250 from  $4.3 \mu\text{g m}^{-3}$  at 6:00 local time (LT) to  $10.4 \mu\text{g m}^{-3}$  at 14:00 LT in 8 h, with the maximum  
251 phochem-SOA mass fraction in OA reaching 65% at 14:00 LT (Fig. 6c). This high average  
252 growth rate of  $0.8 \mu\text{g m}^{-3} \text{h}^{-1}$  in phochem-SOA corresponded to the high  $O_x$  concentration, high  
253 temperature and strong solar radiation in daytime (Fig. S7). In comparison, the concentrations  
254 and the contributions of other SOA factors decreased continuously from 6:00 to 14:00 LT (Fig.  
255 6c). This result further supports the idea that during the high- $O_x$  period of summer,  
256 photochemistry has significant impacts on SOA formation, especially on phochem-SOA. Note  
257 that the role of photochemistry in the formation of phochem-SOA is not limited to the gas-  
258 phase photochemistry, but the photochemistry can also occur in the aqueous phase (Kuang et  
259 al., 2020). This is the case for P3 in our study, which is discussed further in section 3.3 below.  
260 In addition, the potential transformation from POA factors and fresh SOA factors to phochem-





261 SOA through photochemical oxidation could also noticeably affect OA characteristics such as  
262 oxidation state in summer daytime.

### 263 3.3 Aqueous-phase chemistry

264 The aqueous-phase chemistry has imposed significant impacts on SOA formation during this  
265 field campaign. To further explore the formation mechanism of SOA associated with aqueous-  
266 phase chemistry, the relationships between different OA factors and ALWC were investigated.  
267 During P3, the mass concentration of aq-SOA increased from  $5 \mu\text{g m}^{-3}$  to  $17 \mu\text{g m}^{-3}$ , yet its  
268 fraction showed a particularly pronounced rise from 22.5% to 52% of total OA when ALWC  
269 increased from 0.3 to  $200 \mu\text{g m}^{-3}$  (Fig. 5e and f). Note that the strong correlation between aq-  
270 SOA and ALWC was not only observed in P3. Rather, the time series of aq-SOA and ALWC  
271 were remarkably well correlated throughout the entire campaign ( $R=0.7$ , Fig. S4). This general  
272 correlation further confirms the important role of aqueous-phase chemistry in the formation of  
273 aq-SOA and characterized the aqueous-phase formation of aq-SOA throughout the campaign  
274 rather than only in the high-RH event as shown in section 3.1 earlier. We also found that the  
275 concentration and fraction of aq-SOA became stable when ALWC was  $> 200 \mu\text{g m}^{-3}$ , which is  
276 probably attributable to that the aq-SOA formation within droplets was soon outweighed by the  
277 scavenging processes when RH was high enough ( $> 95\%$ ). Fig. 5e shows that the fresh-SOA  
278 has similar increasing trend with aq-SOA as ALWC increased, which suggests that aqueous-  
279 phase chemistry might have also played an important role in the formation of fresh-SOA. The  
280 fresh-SOA also increased slightly as  $\text{O}_x$  increased (Fig. 4e), suggesting that both the aqueous-  
281 phase chemistry and the photochemistry (including that in the aqueous phase) participated to  
282 produce fresh-SOA simultaneously.

283 The O:C ratio shows an obvious increase from 0.7 to around 0.85 when ALWC increases to  
284  $200 \mu\text{g m}^{-3}$ , after which it remains relatively stable (0.85) as the ALWC increases further (Fig.  
285 5). These results suggest that aqueous-phase chemistry can affect the oxidation degree of OA  
286 by changing SOA composition, especially the enhanced contribution of aq-SOA. However, the  
287 growth rate of O:C ratios as ALWC increases in P3 was lower than that in P2 (up to 1 as  $\text{O}_x$   
288 increases). Also, the correlation between O:C vs.  $\text{O}_x$  in P2 ( $R= 0.6$ ) was stronger than O:C vs.  
289 ALWC ( $R= 0.3$ ) (Fig. S8). This result illustrates that photochemistry is more efficient in  
290 elevating the oxidation degree of OA than is the aqueous-phase chemistry.

291 Fig. 6e and Fig. 6f illustrate the different types of aqueous-phase chemistry in daytime and  
292 nighttime. The aq-SOA shows a quite clear and unique diurnal pattern in P3, with much higher  
293 mass concentration during the whole day (especially at nighttime) than those in P1 and P2. This  
294 may be attributed to the stagnant meteorological conditions and high RH (thus ALWC), which  
295 facilitated the continuous formation of aq-SOA in P3. During the daytime, the mass



296 concentration of aq-SOA decreased from 6:00 to 16:00 LT, consistent with the decrease of RH  
297 and the increase of temperature (Fig. S7). After 16:00 LT, aq-SOA started to increase from 4.7  
298  $\mu\text{g m}^{-3}$  to 12.7  $\mu\text{g m}^{-3}$  at 6:00 LT, which showed a rapid nighttime growth rate of 0.6  $\mu\text{g m}^{-3}\text{h}^{-1}$   
299 <sup>1</sup>. Higher RH (thus ALWC) and lower temperature were found at nighttime of P3. This likely  
300 indicates that the dark aqueous-phase SOA formation under high-RH conditions was strong  
301 enough to counteract the nighttime scavenging processes. Therefore, the dark aqueous-phase  
302 chemistry forming aq-SOA shows a dominant role (over 40% to OA) during nighttime under  
303 high-RH conditions (P3).

304 In addition, we also noticed that significant photochem-SOA formation also occurred during  
305 daytime in P3 when RH and ALWC were high, with an average growth rate of 0.6  $\mu\text{g m}^{-3}\text{h}^{-1}$ .  
306 This observation is similar to results in a previous study showing that both aqueous-phase and  
307 gas-phase photochemical reactions substantially contributed to the formation of OOA (a  
308 surrogate of SOA) during the high-RH period (Kuang et al., 2020). The rapid daytime photochem-  
309 SOA formation in our study probably occurred in the aqueous phase driven by photochemical  
310 reactions during daytime under humid conditions with high ALWC. Under such high-RH level  
311 (RH > 80%), the water-soluble species produced from photochemistry in the gas phase can also  
312 partition into the aqueous phase and be further oxidized to form low-volatility products (Carlton  
313 et al., 2007; Sullivan et al., 2016). Previous studies have demonstrated that gas-phase oxidants  
314 such as OH radicals and H<sub>2</sub>O<sub>2</sub> can also partition to the aqueous phase to further oxidize  
315 dissolved the oxidized VOCs (OVOCs) into aq-SOA (Ye et al., 2018). Other studies also  
316 suggested that photochemical reactions in the aqueous droplets can occur through direct  
317 photolysis or through oxidation by oxidants (Ervens et al., 2011; 2014; Ye et al., 2018).  
318 Therefore, in our campaign, dark aqueous-phase chemistry played significant roles in rapid aq-  
319 SOA formation during nighttime, while the aqueous-phase photochemistry during daytime  
320 might be responsible for rapid daytime photochem-SOA formation under high-RH conditions  
321 such as during P3. This comparison demonstrates that the nocturnal aqueous-phase chemistry  
322 and daytime aqueous-phase photochemistry were both important pathways in the total SOA  
323 growth.

324 It is worth noting that three peaks were found in the diurnal variation of fresh-SOA in P3.  
325 The peaks at around 6:00 and 19:00 LT were similar to those of aq-SOA, while the peak at  
326 around 13:00 LT corresponded to the peak in the diurnal cycle of O<sub>x</sub> (Fig. 6e). This three-peak  
327 diurnal pattern hints that both the dark aqueous-phase chemistry and the daytime  
328 photochemistry (either in the gas phase or in the aqueous phase) are important in the formation  
329 of fresh-SOA. Our analysis on formation pathways of these SOA factors suggest the potential  
330 interactive roles of gas-phase oxidation, gas-particle partitioning, and aqueous-phase oxidation  
331 in the formation of SOA.



### 332 3.4 SOA from POA transformation

333 The photochemistry and aqueous-phase chemistry show distinct effects on POA evolution  
334 and SOA formation. The relationships between photochem-SOA/aq-SOA and other POA-related  
335 components (HOA + COA + primary-related-SOA) were plotted in Fig. 7. A strong negative  
336 correlation ( $R=-0.8$ ) between POA-related components and photochem-SOA was observed (Fig.  
337 7c), consistent with the decrease in mass concentration of POA-related components during P2.  
338 This observation suggests that the production of photochem-SOA was at least partly facilitated  
339 by photochemical transformation of other OA components. In addition, compared with P1 and  
340 P3, a more positive promotion on the photochem-SOA formation was observed in P2 when  $O_x$   
341 was more than 40 ppb. These observations confirm the results in section 3.2 that intensive  
342 formation of photochem-SOA was not only produced by photochemical oxidation from VOCs at  
343 high- $O_x$  levels, but also potentially through the transformation of POA-related components into  
344 photochem-SOA.

345 In comparison, POA-related components and aq-SOA correlate weakly (Fig. 7b). When  
346 ALWC ( $<20 \mu\text{g m}^{-3}$ ) and nitrate concentrations were lower ( $<3 \mu\text{g m}^{-3}$ ), mostly during P1 and  
347 P2, POA-related components and aq-SOA showed almost no correlation ( $R=0.1$ ). However,  
348 when ALWC concentration and nitrate concentration were higher than those thresholds above  
349 (data points with yellow/red colors mostly during P3), they had a relatively good negative  
350 correlation ( $R= -0.5$ ), indicating the importance of ALWC and nitrate in aqueous-phase  
351 chemistry. This is consistent with results in winter Beijing (Wang et al., 2021), where POA  
352 factor had strong negative correlations with aq-SOA, suggesting that these POA factors might  
353 produce aq-SOA by aqueous-phase oxidation. In addition, under high-ALWC conditions,  
354 nitrate had similar formation mechanisms with aq-SOA or high nitrate supports the potential  
355 formation/transformation from POA-related components to aq-SOA, which is consistent with  
356 the results in section 3.3. The phenomenon of negative correlation between POA-related  
357 components and SOA at high  $O_x$ /ALWC further emphasizes the importance of conversion from  
358 POA to SOA.

359 As shown in the van Krevelen (VK) plot (Fig. 8a), O:C and H:C both increase in the  
360 succession from primary-related-SOA to photochem-SOA and eventually to aq-SOA, supporting  
361 a successive oxidation sequence from primary-related-SOA to aq-SOA. Generally, H:C shows  
362 a decreasing trend as O:C increases for organic compounds during oxidation in other studies  
363 (Ng et al., 2011; Gilardoni et al., 2016; Lee et al., 2017; Zhao et al., 2019; Chen et al., 2021),  
364 suggesting a general negative correlation between H:C and O:C. This positive relationship of  
365 O:C and H:C evolution during oxidative aging in this study is interesting. It might be caused  
366 by ring-breaking reactions which could further promote the transformation of aromatic POA to  
367 aq-SOA. Previous studies in both laboratory (Huang et al., 2018; Wang et al., 2020) and field



368 (Hu et al., 2016a) demonstrated that the OH-initiated ring-breaking reactions of aromatic  
369 species can occur in the aqueous phase and form highly oxidized oxygenated compounds. For  
370 example, Hems and Abbatt (2018) suggested that nitrophenol molecules could react rapidly  
371 with OH radicals in aqueous solutions with the addition of OH functional groups to the aromatic  
372 ring at the initial stage, followed by fragmentation to multifunctional organic species with high  
373 H:C and O:C ratios. Wang et al. (2021) found that the ring-breaking oxidation of aromatic FF-  
374 POA was the mechanism for aq-SOA formation. Similar to those in primary-related-SOA,  
375 PAH-like ions was also found in the mass spectrum of aq-SOA at  $m/z > 150$ , albeit less  
376 pronounced, consistent with a previous study in Beijing (Wang et al., 2021). This is likely due  
377 to the oxidation of PAHs in the conversion of primary-related-SOA and aq-SOA, which is  
378 caused by enhanced hydroxylation of the aromatic ring and increased yields of carboxylic acids  
379 in OH-initiated reactions (Sun et al., 2010). This kind of ring-breaking oxidation of aromatic  
380 POA could thus lead to aq-SOA formation (Huang et al., 2018; Wang et al., 2021).

381 In addition, the locations of aq-SOA and the slope of overall OA are near the line with the  
382 slope of -1 in the VK plot, indicating more carboxylic acid formation while the replacement of  
383 a hydrogen atom with a carboxylic acid group ( $-\text{COOH}$ ) (Heald et al., 2010; Ng et al., 2011).  
384 This observation supports that oxidation of PAHs was probably involved in the conversion of  
385 primary-related-SOA to aq-SOA through aqueous-phase chemistry, leading to  
386 functionalization as carbonyls and carboxylic acids.

#### 387 4. Conclusion

388 The sources and formation mechanisms of SOA were investigated by online aerosol mass  
389 spectrometry and statistical (PMF) analysis from August to September of 2019 in Handan, a  
390 mid-sized industrialized city in NCP of China. Four specific SOA factors were resolved,  
391 including aq-SOA (15% to total OA), phochem-SOA (31%), fresh-SOA (18%) and primary-  
392 related-SOA (5%). By studying the formation of these SOA factors in different selected periods  
393 (P1-P3) against  $\text{O}_x$  and ALWC, we found multiple pathways leading to their formation,  
394 sometimes with mixed pathways for one type of SOA.

395 Both photochemistry and aqueous-phase chemistry resulted in enhanced OA oxidation state,  
396 but the effect of photochemistry was stronger in SOA formation. During high- $\text{O}_x$  period,  
397 photochemistry had imposed significant impacts on the formation and evolution of SOA in  
398 summertime. The phochem-SOA contributed up to 65% to total OA in the daytime, with a high  
399 average growth rate of  $0.8 \mu\text{g m}^{-3} \text{h}^{-1}$ , suggesting the efficient daytime formation of SOA from  
400 photochemistry. Rapid increases of the concentration and contribution (up to 61%) of phochem-  
401 SOA were found as  $\text{O}_x$  increased, while all the other OA factors showed decreasing trends with  
402  $\text{O}_x$  concentration increasing. The difference suggests enhanced secondary transformation from



403 POA/fresh SOA factors to the more aged photochem-SOA under high-O<sub>x</sub> condition. However,  
404 during the high-RH period, two types of aqueous-phase chemistry were both important  
405 pathways for the SOA growth. During nighttime and under high-RH conditions, dark aqueous-  
406 phase chemistry played significant roles with rapid aq-SOA formation (up to 45% in total OA),  
407 while the aqueous-phase photochemistry was more important by rapid photochem-SOA  
408 formation during daytime (up to 39% in total OA). The primary-related-SOA was evidently  
409 linked to the POA originated from coal combustion activities, as indicated by the PAH-like ion  
410 peaks. Although it constituted a small fraction of 5%, the potential transformation and  
411 conversion from primary-related-SOA to aq-SOA could also be an important pathway via  
412 hydroxylation of the aromatic ring or ring-breaking oxidation of aromatic POA species through  
413 aqueous-phase chemistry. This study highlights the multiple reaction pathways, on top of  
414 multiple precursor types, on the SOA formation in industrialized regions, and calls for more  
415 in-depth study on the interactive roles of those formation pathways.

416

417 **Data availability.** Raw data used in this study are archived at the Institute of Earth  
418 Environment, Chinese Academy of Sciences, and are available on request by contacting the  
419 corresponding author.

420 **Supplement.** The Supplement related to this article is available online.

421 **Competing interests.** The authors declare that they have no conflict of interest.

422 **Author contributions.** RJH designed the study. Data analysis and source apportionment were  
423 done by YFG and RJH. YFG and RJH wrote the manuscript. YFG and RJH interpreted data  
424 and prepared display items. All authors commented on and discussed the manuscript.

#### 425 **Acknowledgement**

426 This work was supported by the National Natural Science Foundation of China (no.  
427 41925015), the Key Research Program of Frontier Sciences from the Chinese Academy of  
428 Sciences (no. ZDBS-LY-DQC001), the Strategic Priority Research Program of the Chinese  
429 Academy of Sciences (no. XDB40000000), and SKLLQG (no. SKLLQGTD1801).

430



431 **References**

- 432 An, Z., Huang, R. J., Zhang, R., Tie, X., Li, G., Cao, J., Zhou, W., Shi, Z., Han, Y., Gu, Z.,  
433 and Ji, Y.: Severe haze in northern China: A synergy of anthropogenic emissions and  
434 atmospheric processes, *Proc. Natl. Acad. Sci. U. S. A.*, 116, 8657–8666,  
435 <https://doi.org/10.1073/pnas.1900125116>, 2019.
- 436 Bikkina, S., Kawamura, K., and Sarin, M.: Secondary Organic Aerosol Formation over  
437 Coastal Ocean: Inferences from Atmospheric Water-Soluble Low Molecular Weight Organic  
438 Compounds, *Environ. Sci. Technol.*, 51, 4347–4357, <https://doi.org/10.1021/acs.est.6b05986>,  
439 2017.
- 440 Canagaratna, M. R., Jimenez, J. L., Kroll, J. H., Chen, Q., Kessler, S. H., Massoli, P.,  
441 Hildebrandt Ruiz, L., Fortner, E., Williams, L. R., Wilson, K. R., Surratt, J. D., Donahue, N.  
442 M., Jayne, J. T., and Worsnop, D. R.: Elemental ratio measurements of organic compounds  
443 using aerosol mass spectrometry: Characterization, improved calibration, and implications,  
444 *Atmos. Chem. Phys.*, 15, 253–272, <https://doi.org/10.5194/acp-15-253-2015>, 2015.
- 445 Canonaco, F., Crippa, M., Slowik, J. G., Baltensperger, U., and Prévôt, A. S. H.: SoFi, an  
446 IGOR-based interface for the efficient use of the generalized multilinear engine (ME-2) for  
447 the source apportionment: ME-2 application to aerosol mass spectrometer data, *Atmos. Meas.  
448 Tech.*, 6, 3649–3661, <https://doi.org/10.5194/amt-6-3649-2013>, 2013.
- 449 Carlton, A. G., Turpin, B. J., Altieri, K. E., Seitzinger, S., Reff, A., Lim, H. J., and Ervens, B.:  
450 Atmospheric oxalic acid and SOA production from glyoxal: Results of aqueous  
451 photooxidation experiments, *Atmos. Environ.*, 41, 7588–7602,  
452 <https://doi.org/10.1016/j.atmosenv.2007.05.035>, 2007.
- 453 Chen, W., Ye, Y., Hu, W., Zhou, H., Pan, T., Wang, Y., Song, W., Song, Q., Ye, C., Wang,  
454 C., Wang, B., Huang, S., Yuan, B., Zhu, M., Lian, X., Zhang, G., Bi, X., Jiang, F., Liu, J.,  
455 Canonaco, F., Prevot, A. S. H., Shao, M., and Wang, X.: Real-time characterization of aerosol  
456 compositions, sources and aging processes in Guangzhou during PRIDE-GBA 2018  
457 campaign, *J. Geophys. Res. Atmos.*, <https://doi.org/10.1029/2021jd035114>, 2021.
- 458 Cohen, A. J., Brauer, M., Burnett, R., Anderson, H. R., Frostad, J., Estep, K., Balakrishnan,  
459 K., Brunekreef, B., Dandona, L., Dandona, R., Feigin, V., Freedman, G., Hubbell, B., Jobling,  
460 A., Kan, H., Knibbs, L., Liu, Y., Martin, R., Morawska, L., Pope, C. A., Shin, H., Straif, K.,  
461 Shaddick, G., Thomas, M., van Dingenen, R., van Donkelaar, A., Vos, T., Murray, C. J. L.,  
462 and Forouzanfar, M. H.: Estimates and 25-year trends of the global burden of disease  
463 attributable to ambient air pollution: an analysis of data from the Global Burden of Diseases  
464 Study 2015, *Lancet*, 389, [https://doi.org/10.1016/S0140-6736\(17\)30505-6](https://doi.org/10.1016/S0140-6736(17)30505-6), 2017.
- 465 Donahue, N. M., Robinson, A. L., Stanier, C. O., and Pandis, S. N.: Coupled partitioning,  
466 dilution, and chemical aging of semivolatile organics, *Environ. Sci. Technol.*, 40,  
467 <https://doi.org/10.1021/es052297c>, 2006.



- 468 Duan, J., Huang, R. J., Gu, Y., Lin, C., Zhong, H., Wang, Y., Yuan, W., Ni, H., Yang, L.,  
469 Chen, Y., Worsnop, D. R., and O'Dowd, C.: The formation and evolution of secondary  
470 organic aerosol during summer in Xi'an: Aqueous phase processing in fog-rain days, *Sci.*  
471 *Total Environ.*, 756, 144077, <https://doi.org/10.1016/j.scitotenv.2020.144077>, 2021.
- 472 Dzepina, K., Arey, J., Marr, L. C., Worsnop, D. R., Salcedo, D., Zhang, Q., Onasch, T. B.,  
473 Molina, L. T., Molina, M. J., and Jimenez, J. L.: Detection of particle-phase polycyclic  
474 aromatic hydrocarbons in Mexico City using an aerosol mass spectrometer, *Int. J. Mass*  
475 *Spectrom.*, 263, 152–170, <https://doi.org/10.1016/j.ijms.2007.01.010>, 2007.
- 476 Elser, M., Huang, R., Wolf, R., Slowik, J. G., Wang, Q., Canonaco, F., Li, G., Bozzetti, C.,  
477 Daellenbach, K. R., Huang, Y., Zhang, R., Li, Z., Cao, J., Baltensperger, U., El-haddad, I.,  
478 and Prévôt, A. S. H.: New insights into PM<sub>2.5</sub> chemical composition and sources in two  
479 major cities in China during extreme haze events using aerosol mass spectrometry, 3207–  
480 3225, <https://doi.org/10.5194/acp-16-3207-2016>, 2016.
- 481 Ervens, B., Turpin, B. J., and Weber, R. J.: Secondary organic aerosol formation in cloud  
482 droplets and aqueous particles (aqSOA): A review of laboratory, field and model studies,  
483 *Atmos. Chem. Phys.*, 11, 11069–11102, <https://doi.org/10.5194/acp-11-11069-2011>, 2011.
- 484 Ervens, B., Armin, S., B., L. Y., and J., and T. B.: Key parameters controlling OH-initiated  
485 formation of secondary organic aerosol in the aqueous phase (aqSOA), *J. Geophys. Res.*,  
486 6578–6595, <https://doi.org/10.1002/2013JD021021>. Received, 2014.
- 487 Fountoukis, C. and Nenes, A.: ISORROPIAII: A computationally efficient thermodynamic  
488 equilibrium model for K<sup>+</sup>-Ca<sup>2+</sup>-Mg<sup>2+</sup>-NH<sub>4</sub><sup>+</sup>-Na<sup>+</sup>-SO<sub>4</sub><sup>2-</sup>-NO<sub>3</sub><sup>-</sup>-Cl<sup>-</sup>-H<sub>2</sub>O aerosols, *Atmos.*  
489 *Chem. Phys.*, 7, 4639–4659, <https://doi.org/10.5194/acp-7-4639-2007>, 2007.
- 490 Gilardoni, S., Massoli, P., Paglione, M., Giulianelli, L., Carbone, C., Rinaldi, M., Decesari,  
491 S., Sandrini, S., Costabile, F., and Gobbi, G. P.: Direct observation of aqueous secondary  
492 organic aerosol from biomass-burning emissions, *Proc. Natl. Acad. Sci. U. S. A.*, 113, 10013–  
493 10018, <https://doi.org/10.1073/pnas.1602212113>, 2016.
- 494 Gu, Y., Huang, R. J., Li, Y., Duan, J., Chen, Q., Hu, W., Zheng, Y., Lin, C., Ni, H., Dai, W.,  
495 Cao, J., Liu, Q., Chen, Y., Chen, C., Ovadnevaite, J., Ceburnis, D., and O'Dowd, C.:  
496 Chemical nature and sources of fine particles in urban Beijing: Seasonality and formation  
497 mechanisms, *Environ. Int.*, 140, 105732, <https://doi.org/10.1016/j.envint.2020.105732>, 2020.
- 498 Heald, C. L., Kroll, J. H., Jimenez, J. L., Docherty, K. S., Decarlo, P. F., Aiken, A. C., Chen,  
499 Q., Martin, S. T., Farmer, D. K., and Artaxo, P.: A simplified description of the evolution of  
500 organic aerosol composition in the atmosphere, *Geophys. Res. Lett.*, 37,  
501 <https://doi.org/10.1029/2010GL042737>, 2010.
- 502 Hems, R. F. and Abbatt, J. P. D.: Aqueous Phase Photo-oxidation of Brown Carbon  
503 Nitrophenols: Reaction Kinetics, Mechanism, and Evolution of Light Absorption, *ACS Earth*  
504 *Sp. Chem.*, 2, 225–234, <https://doi.org/10.1021/acsearthspacechem.7b00123>, 2018.





- 505 Hennigan, C. J., Izumi, J., Sullivan, A. P., Weber, R. J., and Nenes, A.: A critical evaluation  
506 of proxy methods used to estimate the acidity of atmospheric particles, *Atmos. Chem. Phys.*,  
507 15, 2775–2790, <https://doi.org/10.5194/acp-15-2775-2015>, 2015.
- 508 Herndon, S. C., Onasch, T. B., Wood, E. C., Kroll, J. H., Canagaratna, M. R., Jayne, J. T.,  
509 Zavala, M. A., Knighton, W. B., Mazzoleni, C., Dubey, M. K., Ulbrich, I. M., Jimenez, J. L.,  
510 Seila, R., de Gouw, J. A., de Foy, B., Fast, J., Molina, L. T., Kolb, C. E., and Worsnop, D. R.:  
511 Correlation of secondary organic aerosol with odd oxygen in Mexico City, *Geophys. Res.*  
512 *Lett.*, 35, <https://doi.org/10.1029/2008GL034058>, 2008.
- 513 Hu, W., Hu, M., Hu, W. W., Niu, H., Zheng, J., Wu, Y., Chen, W., Chen, C., Li, L., Shao, M.,  
514 Xie, S., and Zhang, Y.: Characterization of submicron aerosols influenced by biomass  
515 burning at a site in the Sichuan Basin, southwestern China, *Atmos. Chem. Phys.*, 16, 13213–  
516 13230, <https://doi.org/10.5194/acp-16-13213-2016>, 2016a.
- 517 Hu, W., Hu, M., Hu, W., Jimenez, J. L., Yuan, B., Chen, W., Wang, M., Wu, Y., Chen, C.,  
518 Wang, Z., Peng, J., Zeng, L., and Shao, M.: *Journal of Geophysical Research : Atmospheres*,  
519 1955–1977, <https://doi.org/10.1002/2015JD024020>. Received, 2016b.
- 520 Hu, W., Palm, B. B., Day, D. A., Campuzano-Jost, P., Krechmer, J. E., Peng, Z., De Sa  
521 Suzane, S., Martin, S. T., Alexander, M. L., Baumann, K., Hacker, L., Kiendler-Scharr, A.,  
522 Koss, A. R., De Gouw, J. A., Goldstein, A. H., Seco, R., Sjostedt, S. J., Park, J. H., Guenther,  
523 A. B., Kim, S., Canonaco, F., Prévôt, A. S. H., Brune, W. H., and Jimenez, J. L.: Volatility  
524 and lifetime against OH heterogeneous reaction of ambient isoprene-epoxydiols-derived  
525 secondary organic aerosol (IEPOX-SOA), *Atmos. Chem. Phys.*, 16, 11563–11580,  
526 <https://doi.org/10.5194/acp-16-11563-2016>, 2016c.
- 527 Hu, W., Hu, M., Hu, W., Zheng, J., Chen, C., Wu, Y., and Guo, S.: Seasonal variations in  
528 high time-resolved chemical compositions, sources, and evolution of atmospheric submicron  
529 aerosols in the megacity Beijing, 9979–10000, 2017.
- 530 Huang, D. D., Zhang, Q., Cheung, H. H. Y., Yu, L., Zhou, S., Anastasio, C., Smith, J. D., and  
531 Chan, C. K.: Formation and Evolution of aqSOA from Aqueous-Phase Reactions of Phenolic  
532 Carbonyls: Comparison between Ammonium Sulfate and Ammonium Nitrate Solutions,  
533 *Environ. Sci. Technol.*, 52, 9215–9224, <https://doi.org/10.1021/acs.est.8b03441>, 2018.
- 534 Huang, R. J., Zhang, Y., Bozzetti, C., Ho, K. F., Cao, J. J., Han, Y., Daellenbach, K. R.,  
535 Slowik, J. G., Platt, S. M., Canonaco, F., Zotter, P., Wolf, R., Pieber, S. M., Bruns, E. A.,  
536 Crippa, M., Ciarelli, G., Piazzalunga, A., Schwikowski, M., Abbaszade, G., Schnelle-Kreis,  
537 J., Zimmermann, R., An, Z., Szidat, S., Baltensperger, U., El Haddad, I., and Prévôt, A. S. H.:  
538 High secondary aerosol contribution to particulate pollution during haze events in China,  
539 *Nature*, 514, 218–222, <https://doi.org/10.1038/nature13774>, 2014.
- 540 Huang, R. J., Wang, Y., Cao, J., Lin, C., Duan, J., Chen, Q., Li, Y., Gu, Y., Yan, J., Xu, W.,  
541 Fröhlich, R., Canonaco, F., Bozzetti, C., Ovadnevaite, J., Ceburnis, D., Canagaratna, M. R.,  
542 Jayne, J., Worsnop, D. R., El-Haddad, I., Prevot, A. S. H., and O’Dowd, C. D.: Primary  
543 emissions versus secondary formation of fine particulate matter in the most polluted city





- 544 (Shijiazhuang) in North China, *Atmos. Chem. Phys.*, 19, 2283–2298,  
545 <https://doi.org/10.5194/acp-19-2283-2019>, 2019.
- 546 Huang, R. J., He, Y., Duan, J., Li, Y., Chen, Q., Zheng, Y., Chen, Y., Hu, W., Lin, C., Ni, H.,  
547 Dai, W., Cao, J., Wu, Y., Zhang, R., Xu, W., Ovadnevaite, J., Ceburnis, D., Hoffmann, T.,  
548 and D. O'Dowd, C.: Contrasting sources and processes of particulate species in haze days with  
549 low and high relative humidity in wintertime Beijing, *Atmos. Chem. Phys.*, 20, 9101–9114,  
550 <https://doi.org/10.5194/acp-20-9101-2020>, 2020.
- 551 Jimenez, J. L., Jayne, J. T., Shi, Q., Kolb, C. E., Worsnop, D. R., Yourshaw, I., Seinfeld, J.  
552 H., Flagan, R. C., Zhang, X., Smith, K. A., Morris, J. W., and Davidovits, P.: Ambient aerosol  
553 sampling using the Aerodyne aerosol mass spectrometer, *J. Geophys. Res. Atmos.*, 108, 1–13,  
554 <https://doi.org/10.1029/2001jd001213>, 2003.
- 555 Jimenez, J. L., Canagaratna, M. R., Donahue, N. M., Prevot, A. S. H., Zhang, Q., Kroll, J. H.,  
556 DeCarlo, P. F., Allan, J. D., Coe, H., Ng, N. L., Aiken, A. C., Docherty, K. S., Ulbrich, I. M.,  
557 Grieshop, A. P., Robinson, A. L., Duplissy, J., Smith, J. D., Wilson, K. R., Lanz, V. A.,  
558 Hueglin, C., Sun, Y. L., Tian, J., Laaksonen, A., Raatikainen, T., Rautiainen, J., Vaattovaara,  
559 P., Ehn, M., Kulmala, M., Tomlinson, J. M., Collins, D. R., Cubison, M. J., Dunlea, E. J.,  
560 Huffman, J. A., Onasch, T. B., Alfarra, M. R., Williams, P. I., Bower, K., Kondo, Y.,  
561 Schneider, J., Drewnick, F., Borrmann, S., Weimer, S., Demerjian, K., Salcedo, D., Cottrell,  
562 L., Griffin, R., Takami, A., Miyoshi, T., Hatakeyama, S., Shimonono, A., Sun, J. Y., Zhang, Y.  
563 M., Dzepina, K., Kimmel, J. R., Sueper, D., Jayne, J. T., Herndon, S. C., Trimborn, A. M.,  
564 Williams, L. R., Wood, E. C., Middlebrook, A. M., Kolb, C. E., Baltensperger, U., and  
565 Worsnop, D. R.: Evolution of organic aerosols in the atmosphere, *Science (80-. )*, 326, 1525–  
566 1529, <https://doi.org/10.1126/science.1180353>, 2009.
- 567 Kuang, Y., He, Y., Xu, W., Yuan, B., Zhang, G., Ma, Z., Wu, C., Wang, C., Wang, S., Zhang,  
568 S., Tao, J., Ma, N., Su, H., Cheng, Y., Shao, M., and Sun, Y.: Photochemical Aqueous-Phase  
569 Reactions Induce Rapid Daytime Formation of Oxygenated Organic Aerosol on the North  
570 China Plain, *Environ. Sci. Technol.*, 54, 3849–3860, <https://doi.org/10.1021/acs.est.9b06836>,  
571 2020.
- 572 Lee, A. K. Y., Chen, C. L., Liu, J., Price, D. J., Betha, R., Russell, L. M., Zhang, X., and  
573 Cappa, C. D.: Formation of secondary organic aerosol coating on black carbon particles near  
574 vehicular emissions, *Atmos. Chem. Phys.*, 17, 15055–15067, <https://doi.org/10.5194/acp-17-15055-2017>, 2017.
- 576 Li, H., Zhang, Q., Zhang, Q., Chen, C., Wang, L., Wei, Z., Zhou, S., Parworth, C., Zheng, B.,  
577 Canonaco, F., Prévôt, A. S. H., Chen, P., Zhang, H., Wallington, T. J., and He, K.: Wintertime  
578 aerosol chemistry and haze evolution in an extremely polluted city of the North China Plain:  
579 Significant contribution from coal and biomass combustion, *Atmos. Chem. Phys.*, 17, 4751–  
580 4768, <https://doi.org/10.5194/acp-17-4751-2017>, 2017.
- 581 Middlebrook, A. M., Bahreini, R., Jimenez, J. L., and Canagaratna, M. R.: Evaluation of  
582 composition-dependent collection efficiencies for the Aerodyne aerosol mass spectrometer



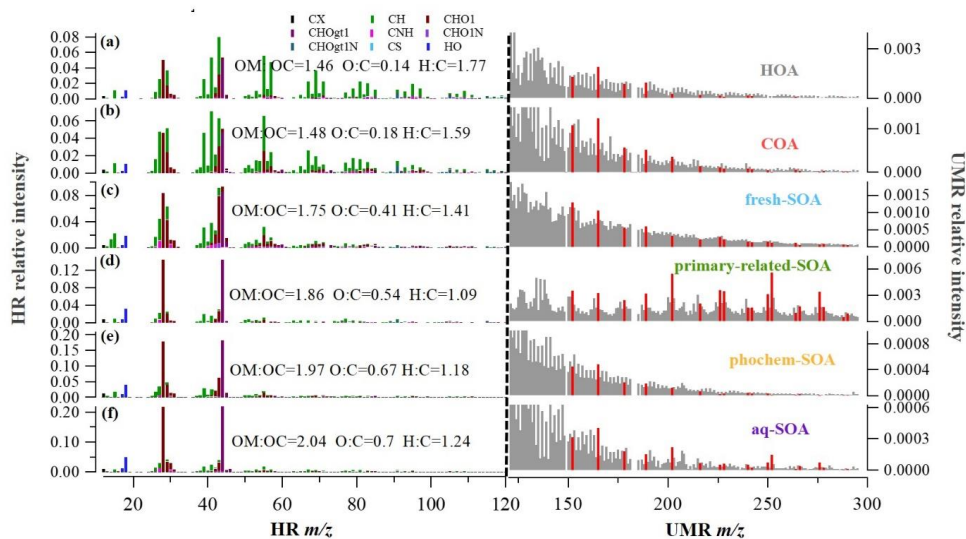
- 583 using field data, *Aerosol Sci. Technol.*, 46, 258–271,  
584 <https://doi.org/10.1080/02786826.2011.620041>, 2012.
- 585 Ng, N. L., Canagaratna, M. R., Jimenez, J. L., Chhabra, P. S., Seinfeld, J. H., and Worsnop,  
586 D. R.: Changes in organic aerosol composition with aging inferred from aerosol mass spectra,  
587 *Atmos. Chem. Phys.*, 11, 6465–6474, <https://doi.org/10.5194/acp-11-6465-2011>, 2011.
- 588 Onasch, T. B., Trimborn, A., Fortner, E. C., Jayne, J. T., Kok, G. L., Williams, L. R.,  
589 Davidovits, P., and Worsnop, D. R.: Soot particle aerosol mass spectrometer: Development,  
590 validation, and initial application, *Aerosol Sci. Technol.*, 46, 804–817,  
591 <https://doi.org/10.1080/02786826.2012.663948>, 2012.
- 592 Paatero, P.: The Multilinear Engine—A Table-Driven, Least Squares Program for Solving  
593 Multilinear Problems, Including the n-Way Parallel Factor Analysis Model, *J. Comput.*  
594 *Graph. Stat.*, 8, 854–888, <https://doi.org/10.1080/10618600.1999.10474853>, 1999.
- 595 Sullivan, A. P., Hodas, N., Turpin, B. J., Skog, K., Keutsch, F. N., Gilardoni, S., Paglione, M.,  
596 Rinaldi, M., Decesari, S., Cristina Facchini, M., Poulain, L., Herrmann, H., Wiedensohler, A.,  
597 Nemitz, E., Twigg, M., and Collett, J. L.: Evidence for ambient dark aqueous SOA formation  
598 in the Po Valley, Italy, *Atmos. Chem. Phys.*, 16, 8095–8108, [https://doi.org/10.5194/acp-16-](https://doi.org/10.5194/acp-16-8095-2016)  
599 8095-2016, 2016.
- 600 Sun, Y., Chen, C., Zhang, Y., Xu, W., Zhou, L., Cheng, X., Zheng, H., Ji, D., Li, J., Tang, X.,  
601 Fu, P., and Wang, Z.: Rapid formation and evolution of an extreme haze episode in Northern  
602 China during winter 2015, 1–9, <https://doi.org/10.1038/srep27151>, 2016.
- 603 Sun, Y., Xu, W., Zhang, Q., Jiang, Q., Canonaco, F., Prévôt, A. S. H., Fu, P., Li, J., Jayne, J.,  
604 Worsnop, D. R., and Wang, Z.: Source apportionment of organic aerosol from 2-year highly  
605 time-resolved measurements by an aerosol chemical speciation monitor in Beijing, China,  
606 *Atmos. Chem. Phys.*, 18, 8469–8489, <https://doi.org/10.5194/acp-18-8469-2018>, 2018a.
- 607 Sun, Y., Xu, W., Zhang, Q., Jiang, Q., Canonaco, F., and Prévôt, A. S. H.: Source  
608 apportionment of organic aerosol from two-year highly time-resolved measurements by an  
609 aerosol chemical speciation monitor in Beijing, China, 2018b.
- 610 Sun, Y. L., Zhang, Q., Anastasio, C., and Sun, J.: Insights into secondary organic aerosol  
611 formed via aqueous-phase reactions of phenolic compounds based on high resolution mass  
612 spectrometry, *Atmos. Chem. Phys.*, 10, 4809–4822, [https://doi.org/10.5194/acp-10-4809-](https://doi.org/10.5194/acp-10-4809-2010)  
613 2010, 2010.
- 614 Wang, J., Ye, J., Zhang, Q., Zhao, J., Wu, Y., Li, J., Liu, D., Li, W., Zhang, Y., Wu, C., Xie,  
615 C., Qin, Y., Lei, Y., Huang, X., Guo, J., Liu, P., Fu, P., Li, Y., Lee, H. C., Choi, H., Zhang, J.,  
616 Liao, H., Chen, M., Sun, Y., Ge, X., Martin, S. T., and Jacob, D. J.: Aqueous production of  
617 secondary organic aerosol from fossil-fuel emissions in winter Beijing haze, *Proc. Natl. Acad.*  
618 *Sci. U. S. A.*, 118, 1–6, <https://doi.org/10.1073/pnas.2022179118>, 2021.
- 619 Wang, S., Newland, M. J., Deng, W., Rickard, A. R., Hamilton, J. F., Muñoz, A., Ródenas,  
620 M., Vázquez, M. M., Wang, L., and Wang, X.: Aromatic Photo-oxidation, A New Source of



- 621 Atmospheric Acidity, *Environ. Sci. Technol.*, 54, 7798–7806,  
622 <https://doi.org/10.1021/acs.est.0c00526>, 2020.
- 623 Xu, S., Liu, W., and Tao, S.: Emission of Polycyclic Aromatic Hydrocarbons in China,  
624 *Biophys. Process. Anthropol. Org. Compd. Environ. Syst.*, 40, 267–281,  
625 <https://doi.org/10.1002/9780470944479.ch11>, 2006.
- 626 Xu, W., Han, T., Du, W., Wang, Q., Chen, C., Zhao, J., Li, J., Fu, P., Wang, Z., Worsnop, D.  
627 R., and Sun, Y.: Effects of Aqueous-phase and Photochemical Processing on Secondary  
628 Organic Aerosol Formation and Evolution in Beijing, China Effects of Aqueous-phase and  
629 Photochemical Processing on Secondary Organic Aerosol Formation and Evolution in  
630 Beijing, China, <https://doi.org/10.1021/acs.est.6b04498>, 2016.
- 631 Xu, W., Sun, Y., Wang, Q., Zhao, J., Wang, J., Ge, X., Xie, C., Zhou, W., Du, W., Li, J., Fu,  
632 P., Wang, Z., Worsnop, D. R., and Coe, H.: Changes in Aerosol Chemistry From 2014 to  
633 2016 in Winter in Beijing: Insights From High-Resolution Aerosol Mass Spectrometry, *J.*  
634 *Geophys. Res. Atmos.*, 124, 1132–1147, <https://doi.org/10.1029/2018JD029245>, 2019.
- 635 Xu, W., Han, T., Du, W., Wang, Q., Chen, C., Zhang, Y., Li, J., Fu, P., Wang, Z., and  
636 Worsnop, D. R.: Supporting Information Effects of Aqueous-phase and Photochemical  
637 Processing on Secondary Organic Aerosol Formation and Evolution in Beijing, China, n.d.
- 638 Ye, C., Liu, P., Ma, Z., Xue, C., Zhang, C., Zhang, Y., Liu, J., Liu, C., Sun, X., and Mu, Y.:  
639 High H<sub>2</sub>O<sub>2</sub> Concentrations Observed during Haze Periods during the Winter in Beijing:  
640 Importance of H<sub>2</sub>O<sub>2</sub> Oxidation in Sulfate Formation, *Environ. Sci. Technol. Lett.*, 5, 757–  
641 763, <https://doi.org/10.1021/acs.estlett.8b00579>, 2018.
- 642 Zhang, Q., Jimenez, J. L., Canagaratna, M. R., Ulbrich, I. M., Ng, N. L., Worsnop, D. R., and  
643 Sun, Y.: Understanding atmospheric organic aerosols via factor analysis of aerosol mass  
644 spectrometry: A review, <https://doi.org/10.1007/s00216-011-5355-y>, 2011.
- 645 Zhao, J., Qiu, Y., Zhou, W., Xu, W., Wang, J., Zhang, Y., Li, L., Xie, C., Wang, Q., Du, W.,  
646 Worsnop, D. R., Canagaratna, M. R., Zhou, L., Ge, X., Fu, P., Li, J., Wang, Z., Donahue, N.  
647 M., and Sun, Y.: Organic Aerosol Processing During Winter Severe Haze Episodes in  
648 Beijing, *J. Geophys. Res. Atmos.*, 124, 10248–10263, <https://doi.org/10.1029/2019JD030832>,  
649 2019.
- 650
- 651
- 652
- 653
- 654



655 **Figures**

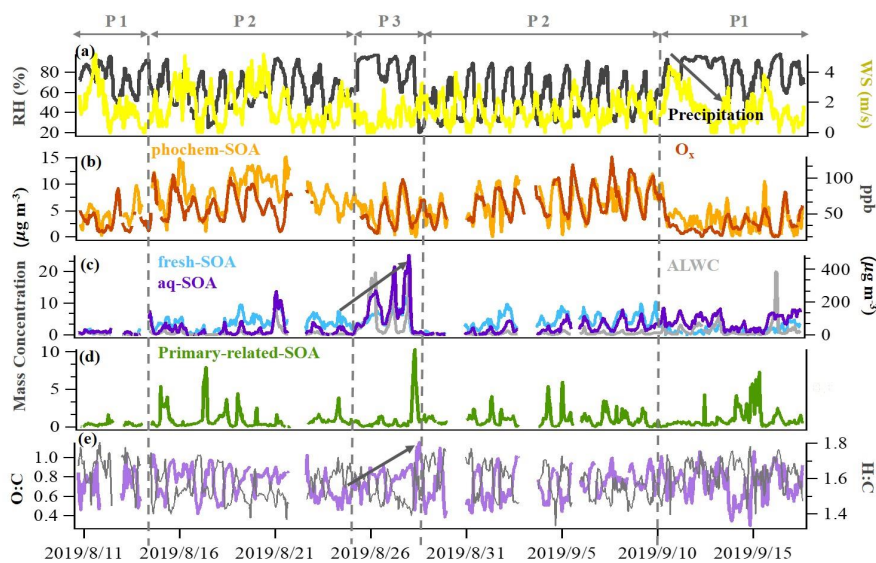


656

657 **Fig. 1** HR and UMR mass spectra of OA factors: (a) HOA; (b) COA; (c) fresh-SOA; (d)  
658 primary-related-SOA; (e) phochem-SOA; (f) aq-SOA. Mass spectra signals less than 120 amu  
659 are colored by nine ion categories, signals equal to or greater than 120 amu are in unit mass  
660 resolution, and polycyclic aromatic hydrocarbons (PAHs) signals are in red on the right panels.

661

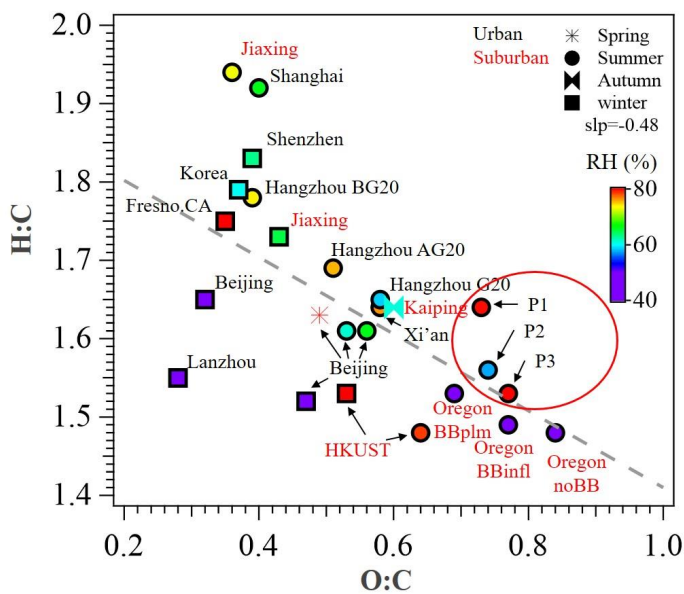
662



663

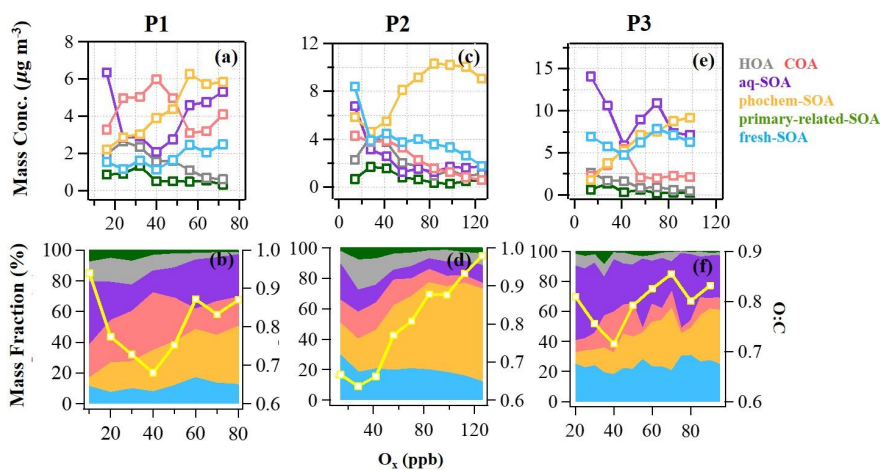
664 **Fig. 2** Time series of (a) relative humidity (RH) and wind speed (WS), (b)  $O_3$  and photochem-  
665 SOA, (c) fresh-SOA, aq-SOA and ALWC, (d) primary-related-SOA, (e) the O:C ratio and H:C  
666 ratio. The time series were categorized to be three typical periods based on total SOA mass  
667 concentrations and meteorology conditions: reference period (P1), high  $O_3$  period (P2) and high  
668 RH period (P3).

669



670

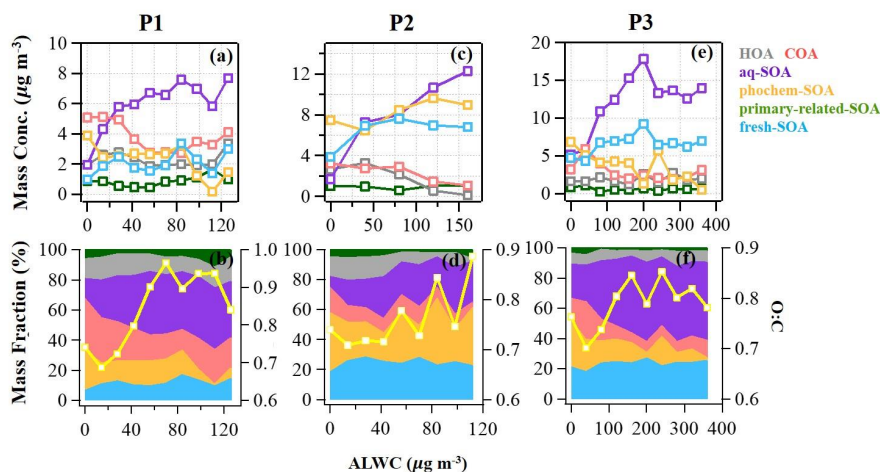
671 **Fig.3** Van Krevelen plot for OA of urban and suburban sites in China and other nations. Data  
 672 points are colored by RH (%). P1, P2 and P3 in red circles represents the different periods in  
 673 this study. All the data and related references can be found in Table S3.



674

675 **Fig. 4** The mass concentration and contribution of OA factors as functions of  $O_x$  in reference  
 676 period (P1: a & b), high  $O_x$  period (P2: c & d) and high RH period (P3: e & f) during this  
 677 campaign. The yellow curves represent the O:C ratio vs.  $O_x$ .

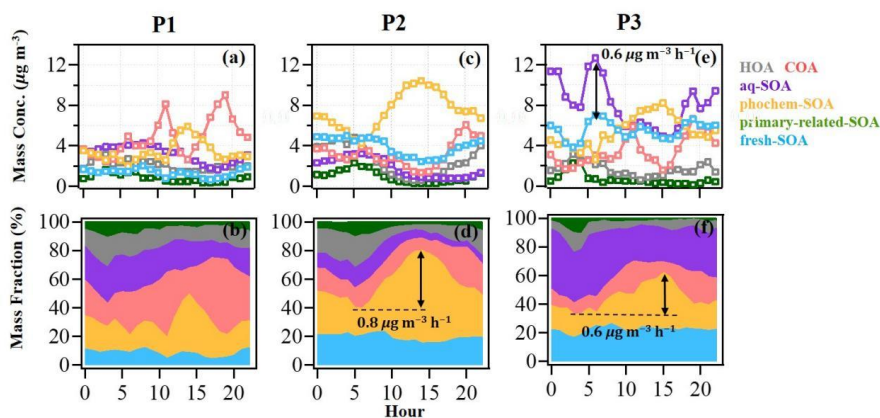




678

679 **Fig. 5** The mass concentration and contribution of OA factors as functions of ALWC in  
680 reference period (P1: a & b), high  $\text{O}_x$  period (P2: c & d) and high RH period (P3: e & f) during  
681 this campaign. The yellow curves represent the O:C ration v.s. ALWC.

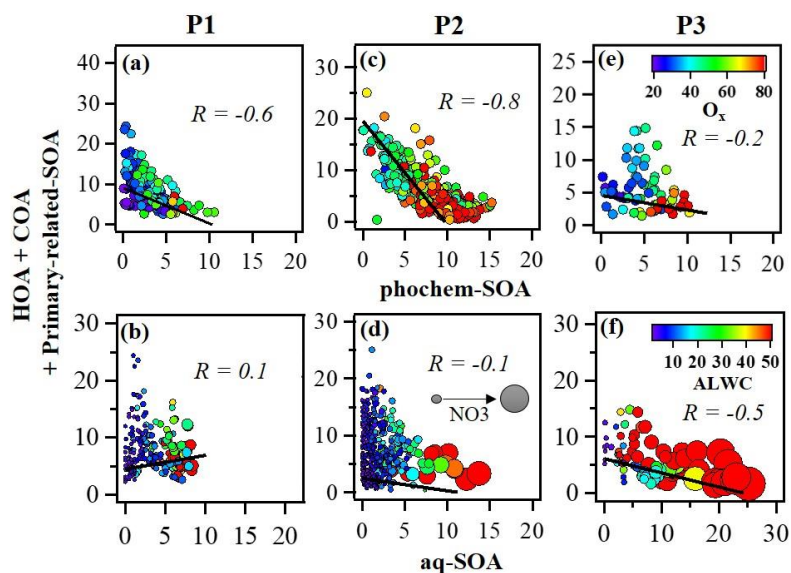
682



683

684 **Fig. 6** Diurnal patterns of mass concentration and mass contribution of OA factors in reference  
685 period (P1: a & b), high  $\text{O}_x$  period (P2: c & d) and high RH period (P3: e & f). The growth rates  
686 of phochem-SOA in P2 and P3 are marked in (d) and (f). The growth rate of aq-SOA in P3 is  
687 marked in (e).

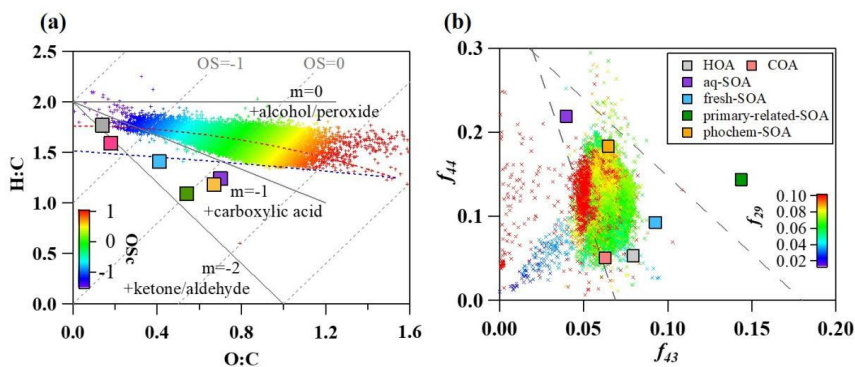
688



689

690 **Fig. 7** Relationship between phochem-SOA and the sum of POA and primary-related-SOA  
 691 colored by  $O_x$  (ppb) in reference period (P1: a), high  $O_x$  period (P2: c) and high RH period (P3:  
 692 e); Relationship between aq-SOA and the sum of POA and primary-related-SOA colored by  
 693 ALWC ( $\mu g m^{-3}$ ) and sized by  $NO_3$  ( $\mu g m^{-3}$ ) in reference period (P1: b), high  $O_x$  period (P2: d)  
 694 and high RH period (P3: f) during this campaign.

695



696

697 **Fig. 8** (a) Van Krevelen diagram for the O:C and H:C ratios of different OA factors (marked  
 698 with squares) and bulk of OA during summer (marked with plus signs and colored by  
 699 Oscarbon oxidation state (OSc)); (b) Triangle plot of  $f_{44}$  versus  $f_{43}$ , the dash lines were adopted  
 700 from Ng et al. (2010) (marked with plus signs and colored by  $f_{29}$ ).